

Corrosion Inhibition Effect of N-(4-diethylaminobenzyl) Quaternary Ammonium Chitosan for X80 Pipeline Steel in Hydrochloric Acid Solution

Ping Li, Liang He*, Xinqi Li, Xinran Liu, Min Sun

School of Materials Engineering, Shanghai University of Engineering Science, Shanghai 201620, China

*E-mail: jljhl@163.com

Received: 4 September 2020 / *Accepted:* 26 October 2020 / *Published:* 30 November 2020

Two water-soluble chitosan derivatives of quaternary amine salt chitosan and N-(4-diethylaminobenzyl) quaternary ammonium chitosan were synthesised, characterised and deployed as corrosion inhibitors for X80 pipeline steel in 1 M hydrochloric acid solution. DAC exhibits better corrosion inhibition performance due to more adsorption centres and more stable adsorption. The potentiodynamic polarization curves revealed that the inhibitors are mixed inhibitors dominated by the anodic reaction. Electrochemical impedance spectroscopy revealed that the corrosion inhibition process is charge-transfer control. The adsorption of inhibitors obeys the Langmuir adsorption isotherm. The thermodynamic parameters of adsorption and surface analysis (SEM, X-ray photoelectron spectroscopy and contact angle) are also discussed.

Keywords: chitosan derivative; corrosion inhibitor; electrochemical; surface analysis; X80 pipeline steel

1. INTRODUCTION

X80 pipeline steel is known for its comprehensive properties such as its high strength and toughness, excellent weldability and processability. It is widely used in the exploitation and transportation of crude oil and natural gas in the oil and gas industry [1-3]. However, X80 pipeline steel would undergo serious corrosion when exposed to acidic environment, which is inevitable in various industrial operations that can result in premature failure. Compared with other corrosion protection measures, such as coating protection, electrochemical protection, corrosion-resistant alloy materials and non-metallic pipes, adding corrosion inhibitor is an effective and relatively cheap method of protecting metal against corrosion.

Amongst the diverse corrosion inhibitors, organic polymer extracts have become the focus of

research; this is due to the fact that they are naturally biodegradable, environment-friendly and renewable. Organic polymer molecules contain N, O, S, P elements, aromatic rings, and C=N bonds with strong electronegative functional groups, which form active adsorption centres and have good corrosion inhibition performance [4]. Examples of organic polymers include *Tabernaemontana contorta* [5]; roses, gardenias, *solanum violaceum* [6]; propolis [7]; maize gluten meals [8]; ginkgo leaves [9]; ficus tikoua leaves [10]; and jasmine tea leaves [11]; all of which have been studied for the inhibition effect.

Chitosan is the product of N-deacetylated chitin, which is commonly found in crab shells, shrimps, arthropods. Chitosan molecules contain a large number of functional groups with active sites: $-NH_2$, $-OH$ and $-COOH$, which provide a lone pair of electrons for iron atoms to form coordination bonds, adsorbing on the metal surface to form a protective film. As a non-toxic, biodegradable organic compound with good film-forming properties, chitosan and its derivatives are used in metal corrosion protection [12-14]. However, the $-NH_2$, $-OH$ and N-acetamide groups in chitosan molecules can form hydrogen bonds within and between molecules, reducing its water solubility and limiting its application. The introduction of hydrophilic groups can effectively reduce the polarity of the chitosan. Quaternary ammonium salt treatment of chitosan can introduce positive charged groups which will effectively improve the water solubility [15] and cation adsorption of the organic compound. The inhibition mechanism of an organic corrosion inhibitor on steel is mainly adsorption, and the introduction of polar atoms or functional groups into chitosan molecules can achieve better adsorption. The $-NH_2$ at the C2 position of chitosan reacts with the active carbonyl in aldehydes to form a highly electronegative imine group ($-C=N$) to form chitosan Schiff base [16, 17]. This will further improve its adsorption with metal surface, which is expected to improve the corrosion inhibition performance.

In this study, water-soluble quaternary amine salt chitosan (QAC) and N-(4-diethylaminobenzyl) quaternary ammonium chitosan (DAC) were synthesized by chitosan. The molecular structures of the synthesized products were characterized by Fourier-transform infrared spectroscopy (FTIR). The weight-loss method, electrochemical analysis method, and surface analysis method were used to investigate the corrosion inhibition efficiency of X80 pipeline steel in 1 M hydrochloric acid solution. The adsorption type and thermodynamic parameters of the inhibitor were also discussed.

2. EXPERIMENTAL

2.1 Materials

The X80 pipeline steel used in the tests has the following chemical composition (in wt. %): C 0.063, Si 0.28, Mn 1.83, Mo 0.22, Ni 0.03, Ti 0.016, Nb 0.061, V 0.059, P 0.011, S 0.0006 and Fe balance. The test samples were cut into cubes with dimensions of 10 mm \times 10 mm \times 3 mm, connected to a copper wire and embedded in epoxy resin with an exposed working area of 1 cm². Before carrying out the electrochemical test, all samples were polished to 2000 grit size with silicon carbide paper, and polished with 1.5 μ m diamond polishing spray. Then, the samples were degreased with acetone, washed with deionised water and finally dried with warm air.

Chitosan (CTS, degree of deacetylation $\geq 90\%$) and glycidyl trimethyl ammonium chloride (GTA, purity $\geq 95\%$) were purchased from Adamas Reagent Co., Ltd, and 4-Diethylaminobenzaldehyde (DEAM, purity $\geq 99.0\%$) was purchased from TCI (Shanghai) Development Co., Ltd. All reagents were analytical reagent grade and were used directly without further purification.

2.2 Synthesis and characterization of chitosan derivatives

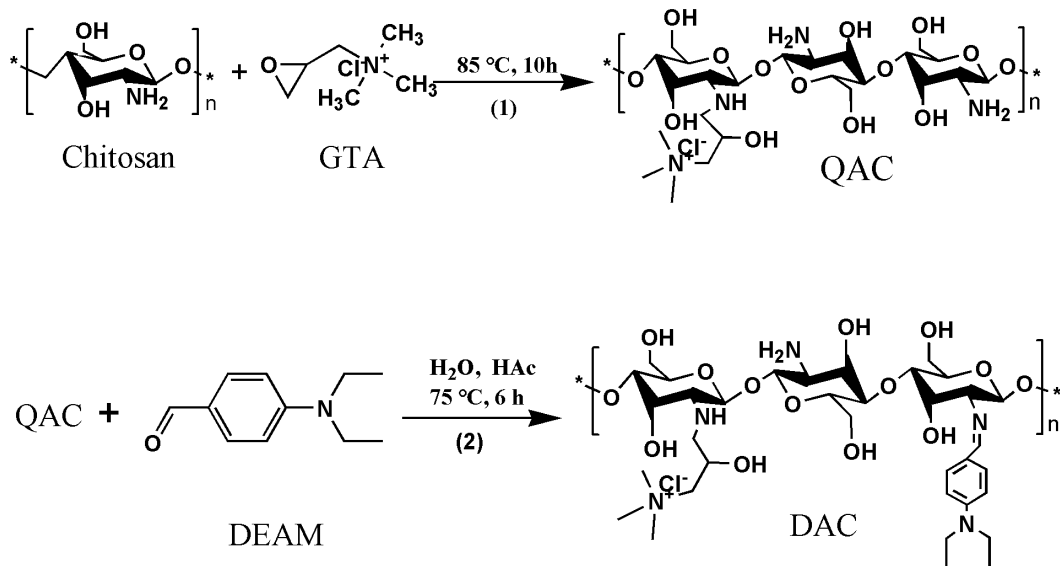


Figure 1. The schematic routes of the synthetic of QAC and DAC.

Two water-soluble chitosan derivatives were synthesized by the route shown in Figure 1. Firstly, the synthesis of QAC was carried out according to the literature [18, 19]. Chitosan (3.0 g) was dissolved in deionized water and stirred at 85 °C for 1 h. Then GTA (6.1 g) was added to the solution, and the mixture was stirred and refluxed for 10 h. After the solution cooled to room temperature, acetone was added to the precipitate. The precipitate was filtered and washed three times with ethanol, dried in a 60 °C vacuum drying oven for 8 h, and finally ground and stored. Secondly, the QAC was dissolved in 20 ml 2 % (wt. %) glacial acetic acid solution and stirred for 30 minutes. Then 25 ml of ethanol was added to the mixed solution. After that, 30 ml ethanol with 2.1 g 4-diethylaminobenzaldehyde (DEAM) dissolved was added and stirred at 75 °C for 6 h and cooled to room temperature. Acetone was added to the reaction solution as a precipitant, and then the precipitate was filtrated, washed with ethanol, and dried in a vacuum at 50 °C. The light-yellow powder DAC was obtained after grinding.

The molecular structures of the synthesised products were characterised using FTIR by Nicolet iS10 in the spectral range 4000–500 cm^{-1} , using the KBr pressing method at room temperature.

2.3 Weight-loss measurements

Weight-loss measurement is a widely used and reliable method to characterise the corrosion rate of samples. The test samples were exposed to a 1 M hydrochloric acid solution in the absence and presence of different concentrations of inhibitors. The samples were immersed for 72 h at 30 °C, then

the residual acid was removed, and the samples were dried. The measurements results were performed three times, and then average values and standard deviations were also reported. The obtained data were used to calculate the corrosion rate (C_R , $\text{mg cm}^{-2} \text{h}^{-1}$), as shown in Equation (1) [20]:

$$C_R = \frac{m_0 - m_i}{At} \quad (1)$$

where m_0 and m_i (mg) are the mass values of the samples before and after immersion, respectively, A is the area that is immersed in the solution (cm^2), and t is the time of exposure (h). The inhibition efficiency (IE_W %) is calculated by using Equation (2):

$$IE_W \% = \frac{C_R^0 - C_R}{C_R^0} \times 100\% \quad (2)$$

where C_R^0 and C_R are the corrosion rates of X80 pipeline steel in the absence and presence of a corrosion inhibitor.

2.4 Electrochemical measurements

Electrochemical measurements were conducted in a traditional three-electrode cell, including working electrode, reference electrode (saturated calomel electrode, SCE), and counter electrode (platinum electrode), respectively. All electrochemical measurements were performed in 1 M hydrochloric acid solution at 30 °C. Before the electrochemical examination, the three-electrode system was immersed in the aggressive solution for about 20 min until the system reached a steady open-circuit potential (E_{OCP}).

The potentiodynamic polarization (PDP) measurements were performed in CHI 770E electrochemical workstation (Chenhua, China). The scanning range of the PDP test was from -250 to $+250$ mV (vs. E_{OCP}), with a scan rate of 1 mV s^{-1} [21]. The electrochemical impedance spectroscopy (EIS) measurements were carried out in Metrohm Autolab B.V. and using the Nova 2.1.3 software for data fitting. The EIS measurements were carried out in the frequency range 100 kHz – 10 mHz , with 10 mV AC signals. The inhibition efficiency of the PDP and EIS measurements (IE_P % and IE_E %) are calculated using Equation (3) and Equation (4):

$$IE_P \% = \frac{I_{corr}^0 - I_{corr}}{I_{corr}^0} \times 100\% \quad (3)$$

$$IE_E \% = \frac{R_{ct} - R_{ct}^0}{R_{ct}} \times 100\% \quad (4)$$

where I_{corr}^0 and I_{corr} indicate the corrosion current densities in the corrosion solution in the absence and presence inhibitor; R_{ct}^0 and R_{ct} represent the charge-transfer resistances in the absence and presence of inhibitor, respectively.

2.5 Surface analysis

The surface corrosion morphology of the samples was obtained using a scanning electron microscope (Hitachi, S-3400, Japan). The morphology was assessed on the samples after their immersion in 1 M hydrochloric acid in the absence and presence of a 6.00 mg L^{-1} chitosan, QAC, and DAC solution for 72 h at 30 °C. The wettability of the above samples' surfaces after immersion was measured by the contact angle tester (SZ-CAM, China).

To investigate the surface elemental composition of the immersed steel, X-ray photoelectron spectroscopy (XPS, Thermo Kalpha, Thermo ESCALAB 250XI) was conducted using a monochromated Al K α X-ray source ($E = 1360$ eV). The XPS survey spectrum and high-resolution spectra were collected with pass energies of 100 eV and 50 eV, respectively. The calibration of the binding energy was performed with C 1s (284.8 eV) peak.

3. RESULTS AND DISCUSSION

3.1 FTIR studies

The FTIR spectra of the chitosan, QAC and DAC are shown in Figure 2.

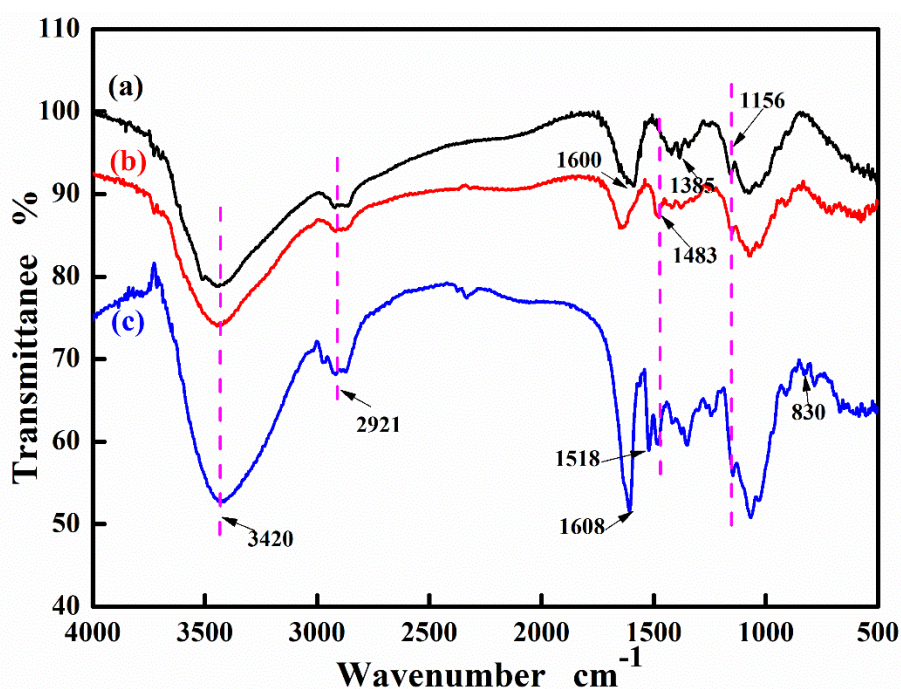


Figure 2. FTIR spectrum of (a) chitosan; (b) QAC and (c) DAC

The wide characteristic peak of the chitosan spectrum observed at 3420 cm^{-1} is attributed to the stretching vibration of the amino and hydroxyl groups. The peak at 2921 cm^{-1} is assigned to the asymmetric vibration of the C-H bond. The peak around 1600 cm^{-1} could be assigned to the characteristic amide II band (N-H) stretching vibration, and the peak at 1385 cm^{-1} can be classified as the stretching vibration of amide III bond (C-N) [22]. The infrared absorption peak at 1156 cm^{-1} is considered to be the asymmetric stretching vibration of C-O-C group [23]. The infrared spectra of QAC and DAC are similar to that of the chitosan. As shown in Figure 2(b), the new absorption peak at 1483 cm^{-1} can be attributed to the bending vibration of the C-H bond, which contains trimethyl amino group due to methylated chitosan quaternary salts [19]. In the spectrum of Figure 2(c), the peak at 1518 cm^{-1} is associated with the stretching vibration of the C=C bond in the aromatic group, and the peak at 830 cm^{-1} shows aromatic ring substitution. The sharp peak at 1608 cm^{-1} is referred to the vibration of the

imine-based C=N group, which indicates that the target product DAC has been successfully synthesized.

3.2 Weight-loss studies

The weight-loss test is a classical method to determine the corrosion rate of metals, and it is the most reliable method to evaluate the average corrosion [24]. The statistical data of the corrosion rate (C_R) and inhibition efficiency (IE_W %) on weight-loss results for X80 pipeline steel are given in Figure 3. From the results, the corrosion rate of the samples is seen to reduce considerably with inhibitors adding. It appears from the results in Figure 3 that DAC is a better steel inhibitor than QAC, which exhibits a higher inhibition efficiency than chitosan. When the concentration of the inhibitors was lower than 10.00 mg L^{-1} , the inhibition efficiency significantly increased with the inhibitors' concentration. This can be explained by the inhibitor molecules adsorbed on the steel surface to form a protective film, reducing the exposure of active sites [25].

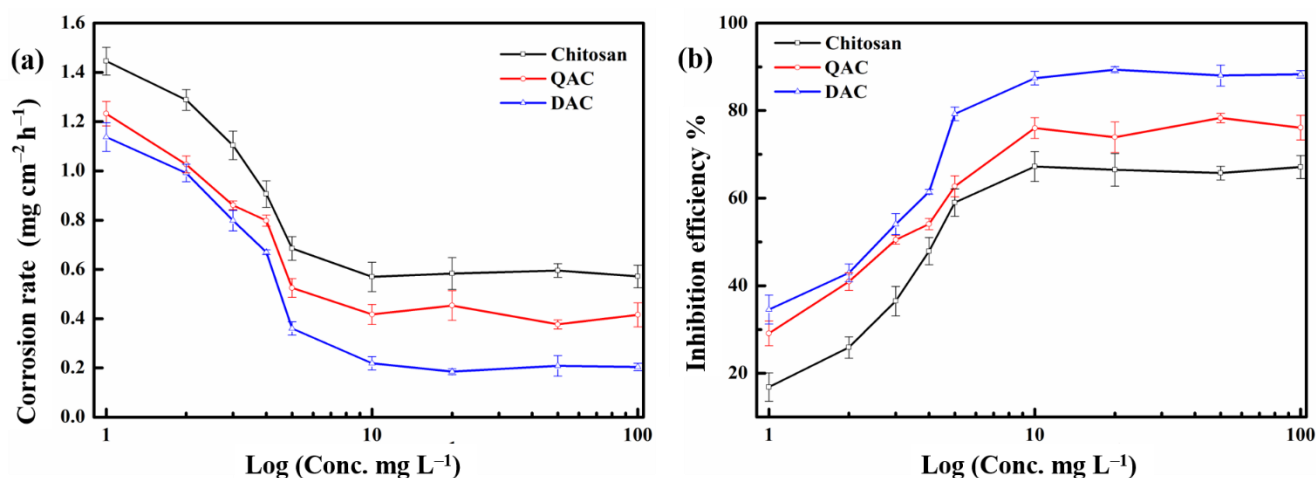


Figure 3. Statistical results of weight loss test for X80 pipeline steel in a 1 M hydrochloric acid solution in the absence and presence of different concentrations of inhibitors at 30 °C for 72h: (a) corrosion rate; (b) inhibitor efficiency.

As the concentration increased to more than 10.00 mg L^{-1} , there were no evident changes in the corrosion inhibition efficiency. This result may be explained by the fact that the inhibitor molecule reaches the dynamic equilibrium state of adsorption-desorption at about 10.00 mg L^{-1} . When the concentration of the inhibitors reached 10.00 mg L^{-1} , the maximum inhibition efficiencies of the chitosan, QAC and DAC were 67.23 %, 76.01 %, and 87.41 %, respectively.

3.3 Potentiodynamic polarisation studies

Potentiodynamic polarisation measurement was carried out to further explore the kinetic

information of cathodic and anodic reactions in the corrosion process. The effect of the inhibitors and concentration are demonstrated in Figure 4. Table 1 shows the electrochemical parameters derived from the PDP plots, including the anodic and cathodic slopes (β_a , β_c), polarisation resistance (R_p), corrosion potential (E_{corr}), and corrosion current density (j_{corr}).

Table 1. Potentiodynamic polarization parameters of X80 pipeline steel in 1 M hydrochloric acid in the absence and presence of various concentrations of chitosan, QAC and DAC.

Inhibitor	Conc. mg L ⁻¹	$-\beta_c$ mV dec ⁻¹	β_a mV dec ⁻¹	R_p Ω cm ²	E_{corr} mV	j_{corr} μ A cm ⁻²	
Blank	-	129	111	25.9	-459	998.9	-
Chitosan	1.00	114	82	40.8	-441	510.0	48.94
	2.00	116	74	49.6	-439	396.0	60.36
	3.00	113	73	53.4	-438	361.9	63.77
	4.00	111	70	59.8	-436	312.5	68.72
	5.00	115	80	71.9	-439	285.9	71.38
	10.00	115	69	63.0	-439	296.4	70.33
	20.00	109	70	62.2	-444	297.5	70.21
	50.00	119	71	66.9	-439	290.0	70.97
QAC	100.00	145	116	92.8	-440	302.3	69.74
	1.00	108	72	56.3	-434	334.2	66.54
	2.00	103	72	81.6	-424	226.2	77.36
	3.00	107	61	142.0	-420	118.2	88.17
	4.00	108	61	179.4	-430	94.2	90.57
	5.00	113	60	185.0	-428	91.9	90.80
	10.00	118	55	316.4	-434	51.7	93.66
	20.00	122	64	148.6	-443	122.6	87.72
DAC	50.00	172	148	288.4	-446	120.1	87.97
	100.00	119	71	157.8	-441	122.1	87.78

Inhibitor	Conc. mg L ⁻¹	$-\beta_c$ mV dec ⁻¹	β_a mV dec ⁻¹	R_p Ω cm ²	E_{corr} mV	j_{corr} μ A cm ⁻²	
	2.00	107	81	93.5	-446	214.7	78.51
	3.00	104	71	142.7	-448	128.5	87.14
	4.00	114	69	237.5	-454	78.4	92.15
	5.00	113	67	243.2	-455	74.8	92.51
	10.00	117	53	436.0	-439	36.5	96.34
	20.00	123	67	218.2	-449	86.2	91.37
	50.00	132	68	198.0	-450	98.6	90.12
	100.00	125	68	246.2	-445	77.9	92.20

The anode region represents the dissolution reaction of the metal, and the cathode region represents the reduction of H⁺ to hydrogen. There is a clear trend that the current corrosion densities of the anode and cathode regions decrease as the concentration of the inhibitor increases. In addition, the values of β_c and β_a do not change significantly for the absence and present of inhibitors. As shown in Figure 4, the cathode branches of the polarization curve are in a nearly parallel arrangement. This indicates that the cathode reaction rate is limited and the dissolution rate of steel is reduced, but the type of reaction does not change [26-28]. However, in the presence of inhibitors, the E_{corr} slightly shifts to the positive direction, but the shift deviation of E_{corr} to positive potential is less than 85 mV, suggesting that the chitosan, QAC and DAC are mixed-type inhibitors which are mainly dominated by the anode reaction [13, 29].

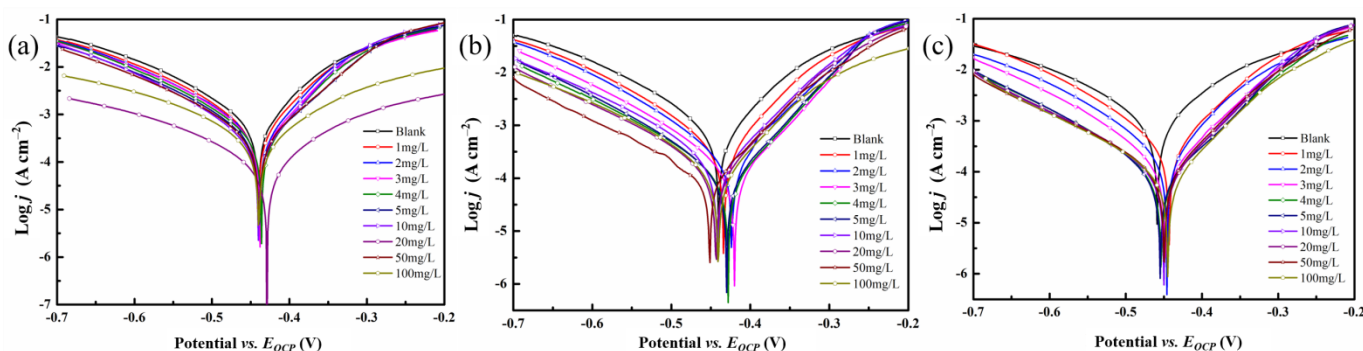


Figure 4. Typical potentiodynamic polarization curves of X80 pipeline steel in a 1 M hydrochloric acid solution with different inhibitors at 30 °C, (a) chitosan, (b) QAC and (c) DAC.

The corrosion inhibitor efficiencies of the chitosan, QAC and DAC are shown in Figure 4(d). When the concentration of the corrosion inhibitor increases but is lower than 10.00 mg L⁻¹, the corrosion

current density decreases, and the inhibition efficiency increases. However, when the concentration is higher than 10.00 mg L^{-1} , there is no obvious increase in inhibition efficiency. It indicated that the inhibitor molecules on the sample's surface reached adsorption and desorption dynamic equilibrium. This result is consistent with the weight-loss measurement. When the concentration of the chitosan, QAC and DAC in 1 M hydrochloric acid solution is 10.00 mg L^{-1} , the corrosion inhibition efficiency reaches 70.28 %, 93.66 %, and 96.34 %, respectively. Consequently, DAC as a corrosion inhibitor of X80 steel in corrosive medium has a better corrosion inhibition ability.

3.4 Electrochemical impedance spectroscopy studies

EIS is an effective method to study the kinetic process of the interface between electrode and electrolyte. The impedance of X80 pipeline steel in the absence and presence of various concentrations of inhibitors in 1 M hydrochloric acid solution at $30 \text{ }^\circ\text{C}$ was detected, and Nyquist diagrams and Bode plots are given in Figure 5.

As shown in Figure 5(a-c), the Nyquist curves deviated from the perfect semi-circular shape, which was caused by the frequency dispersion due to the roughness and unevenness of the samples' surfaces [30, 31]. The capacitive loop indicated that the dissolution of the metal samples in the corrosive solution is controlled by a charge-transfers process [32]. The radius of the capacitive loops increases with the concentration of the inhibitors, and the shape is almost unchanged. It demonstrated that the corrosion inhibitor only changes the corrosion rate without changing the type of corrosion. The Bode phase plot is shown in Figure 5(d-f), and the phase angle values can measure the roughness of the metal's surface. The phase angle plot has a single peak, which indicates a one-time constant appearing at the metal surface/solution interface in the corrosion process [33]. As the concentration of the corrosion inhibitor increased, the phase angle value moved upwards, which indicated that more inhibitor molecules are adsorbed on the sample's surface [34].

The corresponding electrochemical impedance parameters were analyzed in terms of the equivalent circuit (Figure 5 (g)) which consists of R_s (solution resistance), R_{ct} (the charge-transfer resistance), and CPE (constant phase element). Due to the fact that the electric double layer formed in the electrolyte and the electrode does not have pure capacitor characteristic, the capacitor is substituted by a constant phase element (CPE) [35]. The double-layer capacitance (C_{dl}) is calculated using Equation 5 [30]:

$$C_{dl} = (Y_0 R_{ct}^{1-n})^{\frac{1}{n}} \quad (5)$$

where Y_0 is the constant of the CPE, and n is the index of CPE. The n value, ranging from -1 to 1 , represents the unevenness or roughness of the sample's surface. For $n = 0$, the CPE indicates a resistance, $n = 1$ indicates a pure capacitor, and $n = -1$ indicates inductance [36].

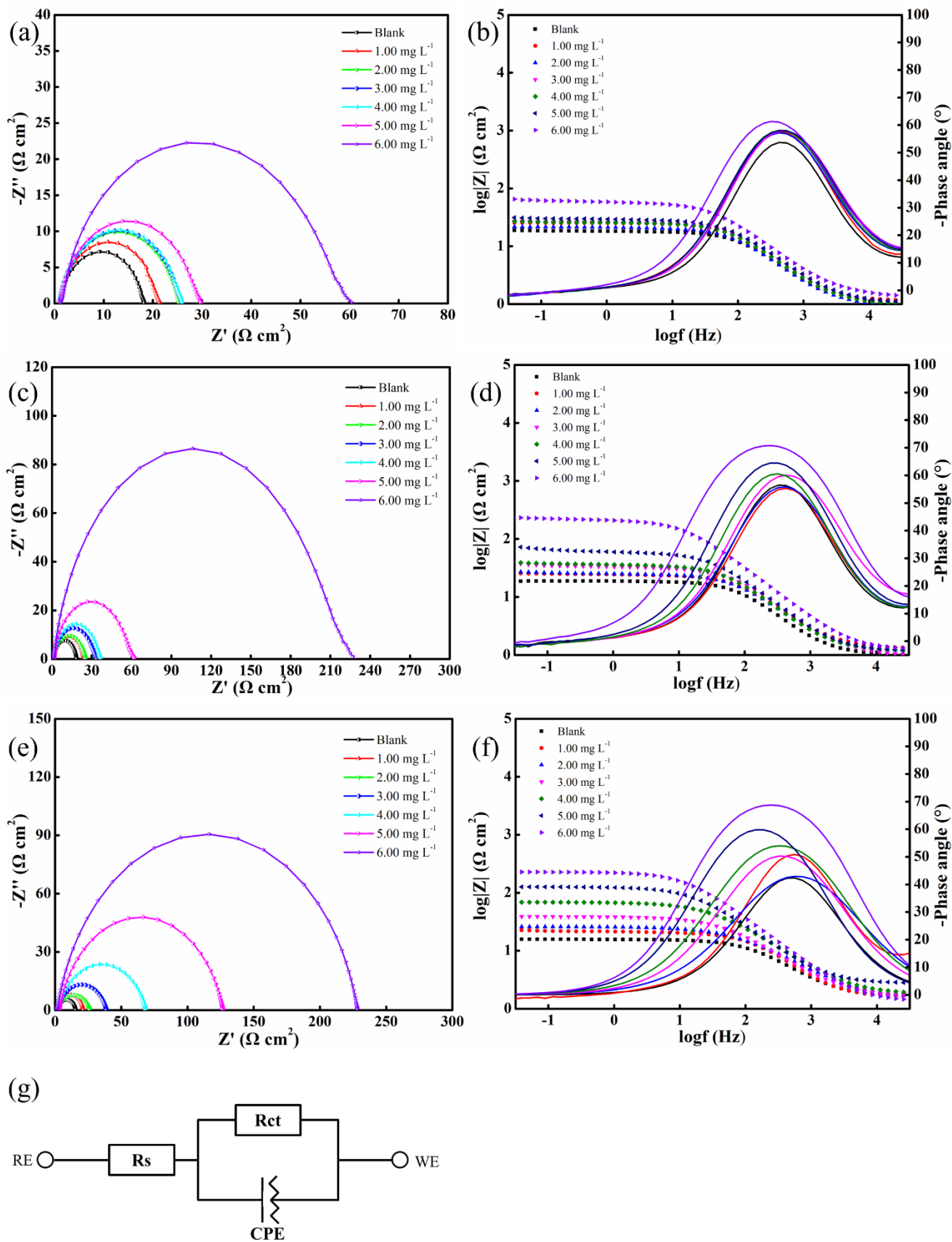


Figure 5. Nyquist diagrams and Bode plots of X80 pipeline steel in 1 M hydrochloric acid solution in the absence and presence of different inhibitors at 30 °C: (a), (b) chitosan; (c), (d) QAC; (e), (f) DAC; and (g) the electrochemical equivalent circuit model.

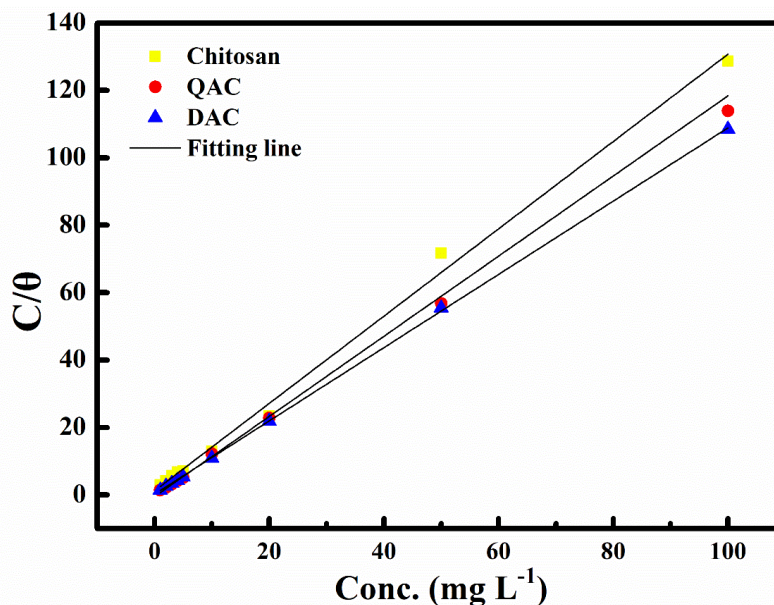


Figure 6. Langmuir adsorption isotherm for adsorption of chitosan, QAC and DAC on the X 80 pipeline steel surface in 1 M hydrochloric acid at 30 °C.

Table 2. EIS parameters of X80 steel in the presence and absence of various concentrations of chitosan, QAC and DAC.

Inhibitor	Conc. mg L ⁻¹	R _s Ω cm ²	Y _o 10 ⁻⁶ Ω ⁻¹ S ⁿ cm ⁻²	n	R _{ct} Ω cm ²	C _{dl} μF cm ⁻²	IE _E %
Chitosan	0.00	1.202	196.2	0.885	17.12	93.6	-
	1.00	0.965	223.1	0.870	20.45	99.6	16.28
	2.00	1.164	187.0	0.881	24.00	89.9	28.67
	3.00	1.020	213.7	0.860	25.33	91.3	32.41
	4.00	1.017	196.6	0.857	25.37	81.1	32.52
	5.00	1.086	201.3	0.850	29.38	81.2	41.73
	6.00	1.352	185.9	0.831	61.78	75.1	72.29
QAC	0.00	1.040	235.4	0.894	17.67	122.8	-
	1.00	1.327	214.6	0.862	23.44	91.9	24.62
	2.00	1.205	242.4	0.855	24.82	101.6	28.81
	3.00	0.987	235.1	0.835	35.07	91.2	49.62

Inhibitor	Conc. mg L ⁻¹	R _s Ω cm ²	Y _o 10 ⁻⁶ Ω ⁻¹ S ⁿ cm ⁻²	n	R _{ct} Ω cm ²	C _{dl} μF cm ⁻²	IE _E %
	4.00	1.213	217.8	0.868	36.91	104.9	52.13
	5.00	1.196	204.0	0.854	67.52	98.2	73.83
	6.00	1.264	115.0	0.867	224.70	65.5	92.14
	0.00	1.699	275.0	0.830	14.19	88.2	-
	1.00	1.683	186.1	0.853	20.10	71.1	29.40
	2.00	1.519	415.3	0.870	24.41	208.6	41.87
DAC	3.00	1.655	320.3	0.880	38.53	175.9	63.17
	4.00	1.812	256.1	0.870	71.58	140.9	80.18
	5.00	2.769	165.1	0.836	126.90	77.4	88.82
	6.00	1.396	105.9	0.857	230.10	56.9	93.83

The corresponding electrochemical impedance parameters are shown in Table 2. There is a clear trend that R_{ct} increases with the corrosion inhibitor's concentration. The increase of R_{ct} values is due to the adsorption of the inhibitor molecules on the electrode's surface, forming protective films, which leads to the increase of the charge-transfer resistance. As a result, the electrochemical charge-transfer process at the electrode-solution interface becomes more difficult. In addition, the reason for the decrease in the double-layer's capacitance (C_{dl}) may be due to the increase in the thickness of the passivation film formed on the steel surface or the decrease in the local dielectric constant [24]. The inhibition efficiency has been summarised in Table 2. It was found that the inhibition efficiency was 72.29 % when the concentration of the chitosan was 6.00 mg L⁻¹. For QAC, the inhibition efficiency increased to 92.14 %, and the inhibition efficiency of DAC reached 93.83 % with the same concentration. The DAC molecules contain aromatic rings with a planar structure, which induce greater interaction with the steel surface, so the inhibition efficiency of DAC is better than those of the chitosan and QAC [32]. It should be mentioned that the electrochemical results are consistent with the weight-loss results.

3.5 Adsorption isotherm

Different adsorption isothermal models, including Langmuir, Freundlich, Frumkin, Temkin, Flory-Huggins, and Bockris-Swinkels are used to study the inhibition mechanism in order to clarify the adsorption mechanism between the inhibitor molecules and the metal surface [7, 37-39].

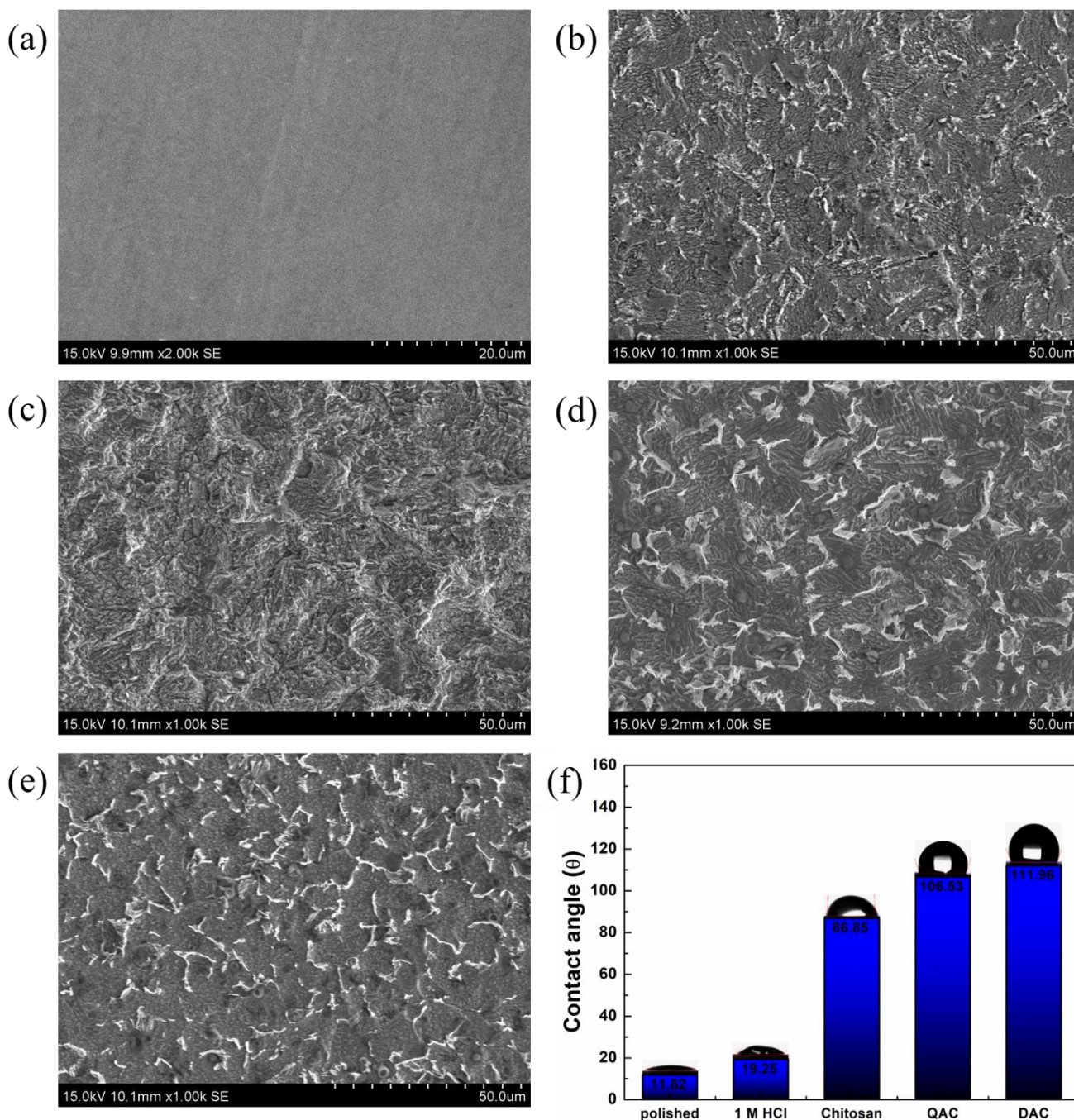


Figure 7. SEM micrographs for (a) polished X80 steel, after immersion for 72 h at 30 °C in (b) 1 M hydrochloric acid, addition 6.00 mg L⁻¹ of (c) chitosan, (d) QAC and (e) DAC, (f) contact angle tests of X80 pipeline steel surface after immersed in different solutions at 30 °C for 72 h.

However, the one which best fitted the experimental data is the Langmuir adsorption isotherm, which is expressed in Equation (6) [40]:

$$\frac{C_{inh}}{\theta} = \frac{1}{K_{ads}} + C_{inh} \tag{6}$$

where C_{inh} is the inhibitor concentration, θ ($\theta = \frac{\eta}{100}$) is the degree of surface coverage calculated by PDP measurements, and K_{ads} is the adsorption equilibrium constant. The results of the PDP test are introduced into Equation (6) to calculate the adsorption equilibrium constant.

The calculated parameters of C_{inh}/θ and C_{inh} are shown in Figure 6.

In order to calculate the adsorption parameters, linear least-squares optimisation is used. The results clearly show that the linear fit of $C_{inh}/\theta-C_{inh}$ is good for the three inhibitors in 1 M hydrochloric acid at 30 °C. The regression coefficient is greater than 0.99, which indicates that the experimental data are in accordance with the Langmuir isotherm. The adsorption-desorption strength between the inhibitor molecules and metal surfaces can be calculated. The Gibbs adsorption free energy (ΔG_{ads}^0) is calculated using Equation (7) [41]:

$$\Delta G_{ads}^0 = -RT \ln(1000K_{ads}) \quad (7)$$

where R is the universal gas constant, T is the thermodynamic temperature (K), and 1000 is the concentration of water molecules expressed in g L^{-1} .

The thermodynamic parameters of adsorption are shown in Table 3.

Table 3. Thermodynamic parameters for the adsorption of chitosan, QAC and DAC on the X80 surface in a 1 M hydrochloric acid at 30 °C.

Inhibitor	Intercept	K_{ads} L mg^{-1}	$-\Delta G_{ads}^0$ kJ mol^{-1}	R^2
Chitosan	1.29	0.81	34.3	0.9964
QAC	1.19	1.59	36.0	0.9994
DAC	1.08	4.42	38.6	0.9999

The negative value of ΔG_{ads}^0 indicates that the process of inhibitor molecules adsorption to the metal surface occurs spontaneously. Generally, the absolute values of ΔG_{ads}^0 reach around 20 kJ mol^{-1} or lower are related to physical adsorption, which is caused by electrostatic interactions between charged molecules and ions on charged metal surfaces. The values around 40 kJ mol^{-1} or higher, however, are related to chemisorption, which is due to the sharing or transfer of electrons in the inhibitor molecules on metal surface to form a coordinate covalent bond [32]. In this study, the ΔG_{ads}^0 values for the chitosan, QAC, and DAC are -34.3 , -36.0 and -38.6 kJ mol^{-1} , indicating that their adsorption type on the metal surface in 1 M hydrochloric acid solution is the result of the combined action of physical and chemical adsorption. It is worth noting that the ΔG_{ads}^0 value of DAC is the most negative, indicating that DAC adsorptivity is stronger than that of chitosan and QAC [42].

3.6 Surface morphology

3.6.1 SEM analysis

The surface corrosion morphology of X80 pipeline steel after immersion was observed by SEM test. As shown in Figure 7(a), the pre-treated surface of X80 pipeline steel is polished with a few

scratches. However, the surface of the steel suffered serious corrosion in 1 M hydrochloric acid solution due to the dissolution of the metal in the strongly acidic solution and the fact that the surface is rough and completely covered by corrosion products (Figure 7(b)). In Figure 7(c-d), the surface of the soaked sample is still covered completely by a rust layer and the average corrosion at different levels is shown. In contrast, as shown in Figure 7(e), the sample surface is smooth and covered with a small amount of corrosion products in the presence of the DAC solution, which clearly demonstrated that DAC has better corrosion inhibition efficiency. A possible explanation for this might be that the passivation film formed on the metal surface hinders chloride ions erosion.

3.6.2 Contact angle analysis

Generally, the anti-corrosion performance of a corrosion inhibitor is related to the hydrophobicity of the inhibitor film [26]. The water contact angle (θ) of a flat and clean polished surface is 11.82° as shown in Figure 7(f). After the sample had been immersed in a 1 M hydrochloric acid solution for 72 h, the θ value was 19.25° due to the presence of hydrophilic corrosion products on the metal surface [43]. In contrast, in the presence of inhibitors, the contact angles obviously increased. The value of the contact angle is closely related to the structure of inhibitor molecules and the properties of substrate surface [40]. When 6.00 mg L^{-1} of chitosan inhibitors was added to the aggressive solution, the value of the contact angle increased to 86.85° , while for the same concentrations of QAC or DAC inhibitors, the contact angles became larger than 90° . This phenomenon can be explained by the formation of hydrophobic protective film on the metal surface. The inhibitor molecules spontaneously bind to Fe atoms in the hydrochloric acid solution and reduce the surface free energy [44, 45]. The DAC molecule contains the hydrophobic group benzene ring and hydrophilic group trimethylaminochloride, which has excellent corrosion inhibition performance in hydrochloric acid.

3.6.3 X-ray photoelectron spectroscopy

The information of the atomic valence and molecular structure of the corrosion products was conducted by XPS. The XPS survey spectra and high-resolution spectra of the sample after immersion in a 1 M hydrochloric acid solution in the absence and presence of 6.00 mg L^{-1} of chitosan and DAC for 24 h are displayed in Figure 8. The binding energy, peak area and atomic ratio of each element are summarized in Table 4. As shown in Figure 8(a), the Cl^- ions are defined as corrodent in the hydrochloric acid solution, while N element is related to corrosion inhibitor films formed on steel surfaces.

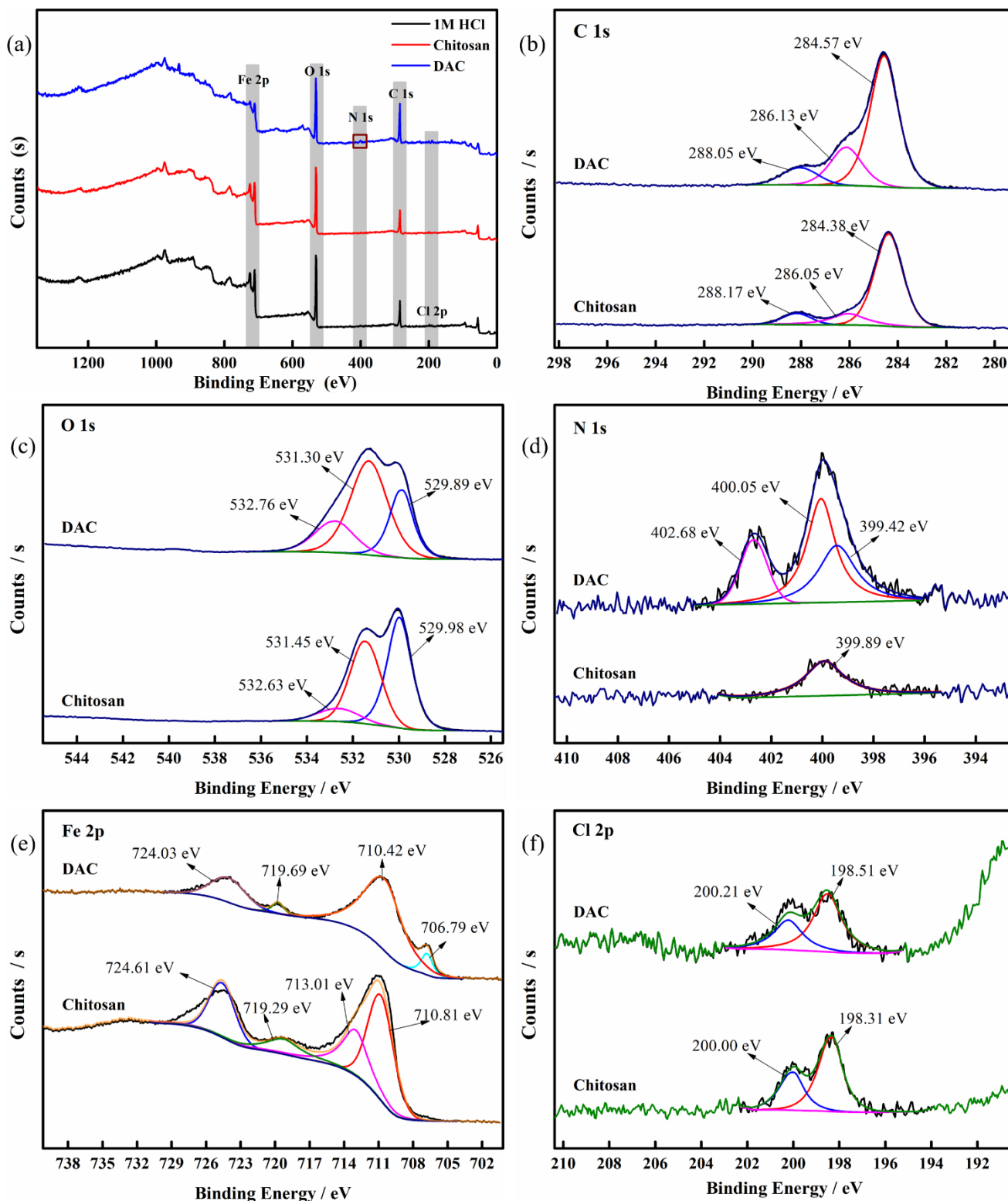


Figure 8. XPS survey spectra and high-resolution spectra of X80 pipeline steel after immersed in 1 M hydrochloric acid absence or presence of 6 mg L⁻¹ DAC at 30 °C for 24 h.

The high-resolution spectra and fitted peaks of each element are shown in Figure 8(b-f), including C 1s, N 1s, O 1s, Fe 2p and Cl 2p. In Figure 8(b), the C 1s (chitosan) spectrum could be deconvoluted

into three peaks: 284.38 eV, 286.05 eV and 288.17 eV, which are attributed to C-C/ C-H, C-N/ C=N and C-OH [46], respectively. Compared to the atomic ratio of C 1s element in Table 4, the atomic ratio of C 1s relatively increased in the presence of the chitosan and DAC inhibitors, which proved that the corrosion inhibitor molecules were adsorbed on the metal [42]. The O 1s (chitosan) spectrum was fitted into three peaks as shown in Figure 8(c). The peaks at 529.98 eV, 531.45 eV and 532.63 eV may be related to two factors: (1). Fe-O bonds in iron oxides (e.g. FeO, Fe₂O₃, Fe₃O₄) which exist on metal surfaces or O²⁻ iron; (2). Hydrated oxides or hydrated iron oxides (FeOOH and /or Fe(OH)₃) present on the metal surface [47]. It is clear from Table 4 that the decrease of corrosion products on the metal surface by adding DAC is the main reason for the rapid drop of O 1s atomic ratio. And this conclusion can also be confirmed by the Fe 2p atomic ratio.

Table 4. Binding energies and atomic ratio of different elements in XPS test for films formed on X80 substrate in 1 M hydrochloric acid.

Element	Without inhibitor			6.00 mg L ⁻¹ Chitosan			6.00 mg L ⁻¹ DAC		
	BE (eV)	Peak area	Atomic ratio (%)	BE (eV)	Peak area	Atomic ratio (%)	BE (eV)	Peak area	Atomic ratio (%)
C 1s	285.08	307016	37.22	285.03	270155	36.35	285.21	476046	51.06
N 1s	-	-	-	399.14	12371	1.07	400.36	30829	2.13
O 1s	530.91	885076	45.38	530.92	816076	44.35	531.22	871024	38.62
Fe 2p	711.44	1538730	18.09	711.48	1281546	16.73	711.13	761169	7.92
Cl 2p	198.24	6635	0.48	198.94	5298	0.34	199.91	4819	0.28

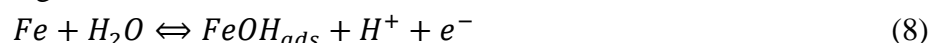
The Fe 2p high-resolution spectrum is deconvoluted into four peaks as shown in Figure 8(e). The peaks at 710.81 eV and 710.42 eV are attributed to Fe oxides, the peak at 713.01 eV could be assigned to FeO and FeOOH, the peaks at 719.29 eV and 719.65 eV are related to FeCl₃, and the peaks at 724.61 eV and 724.03 eV are defined as iron oxides FeOOH, Fe₂O₃ and Fe₃O₄. However, the peak at 706.79 eV in presence of DAC solution is considered as metallic iron, which indicated that the DAC showed a better corrosion inhibition performance [48]. The Cl 2p shows a bimodal profile in Figure 8(f). The binding energies of 198.31 eV and 198.51 eV are related to Cl 2p_{3/2}, while 200.00 eV and 200.21 eV are related to Cl 2p_{1/2} [49], which can be attributed to the Fe-Cl bond which formed FeCl₂ and FeCl₃ on the metal surface. As shown in Table 4, the Cl 2p atomic ratio decreases after adding the inhibitors, which also indicates that less corrosion products are formed.

The N 1s spectrum of various samples are shown in Figure 8(d). For the sample immersed in the corrosive solution with the chitosan inhibitor, only a single peak (399.89 eV) can be detected, which could be assigned to the -NH₂ groups in the chitosan [45]. As for the sample with the DAC inhibitors, the N 1s spectrum can be deconvoluted into three peaks: the first peak at 399.42 eV is attributed to C-N bond and non-protonated =N- structure, and the peaks at 400.05 eV and 402.68 eV represent -NH₂/ -N-Fe groups and protonated N atoms in the DAC molecule [50], respectively. However, no N elements

were detected for the metal sample immersed in a 1 M hydrochloric acid solution without inhibitors. In conclusion, the presence of N element indicates that the inhibitor was adsorbed on the metal surface.

3.7 Corrosion inhibition mechanism

It is well known that organic inhibitor molecules interact with metal surfaces through the adsorption process to achieve the desired anticorrosive purpose; the metal surface is covered, or the active sites are blocked from the aggressive medium by the inhibitor species. The calculated value of K_{ads} suggested that the inhibitors DAC and QAC are adsorbed on the X80 pipeline steel surface through a mixture of chemisorption and physisorption, tending to the former. In a strongly acid solution, the steel acts as a positive electrode which causes a dissolution reaction and renders its surface net positively charged, as shown in the following reactions [27]:



In hydrochloric acid solution, Cl^- ions would be adsorbed on the positively charged steel surface, and steel surface hydrated chloride ions would have excessive negative charges, which is consistent with the XPS analysis.

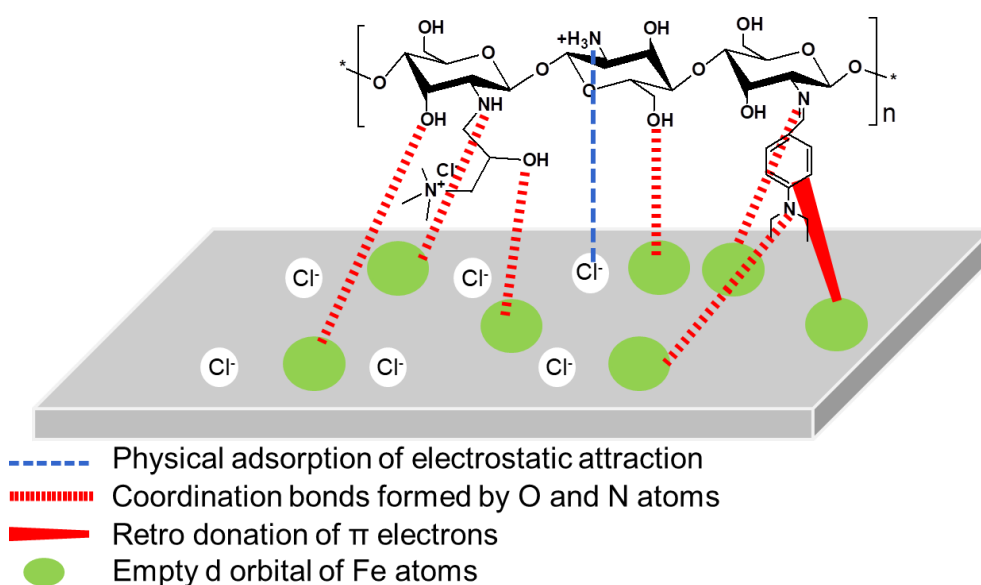


Figure 9. The proposed mechanism of adsorption of DAC on X80 surface exposed to 1 M hydrochloric acid.

The adsorption mechanism of the DAC inhibitor exposed to 1 M hydrochloric acid on the X80 steel surface is shown in Figure 9. Compared with the chitosan inhibitor, the positively charged quaternary ammonium salt functional group present in the QAC molecules greatly increase its polarity and promotes the adsorption between transition metals and corrosion inhibitors. For DAC, except for the

functional groups mentioned in QAC, benzene rings are the new adsorption centers. The π -electrons in the aromatic ring and the empty d orbital of the Fe atoms form a donor-acceptor relationship, which is adsorbed on the metal surfaces to form a passivation film [35, 51]. On the other hand, the protonated species of DAC are adsorbed on the metal surface by electrostatic attraction between the protonated part and the negatively charged chloride ion adsorbed on the metal surface, resulting in physical adsorption. As found in the contact angle measurement, the addition of inhibitor increased the hydrophobicity attributed to the adsorption of inhibitor. The XPS analysis also proved that the lone pair of electrons of N and O atoms form coordination bonds with the 3D empty orbitals of Fe. In summary, in the corrosive solution with the DAC inhibitor, less active sites on the metal surface are exposed to corrosive medium, which consequently proves that DAC inhibitor has a higher inhibition efficiency compared to QAC and chitosan.

4. CONCLUSIONS

The successful synthesis of chitosan derivatives QAC and N-(4-diethylaminobenzyl) quaternary ammonium chitosan (DAC) was achieved. The corrosion resistances of the chitosan, QAC and DAC for X80 pipeline steel in 1 M hydrochloric acid were compared. It has been concluded that the corrosion inhibition efficiency of DAC is better than that of the chitosan and QAC. The surface micromorphology after immersion also supports this conclusion. The thermodynamic calculations confirmed that the type of adsorption on metal surfaces conforms to Langmuir's adsorption isotherm, which includes both physical and chemical adsorption. The increase of the contact angle value on the sample surface confirmed that the hydrophobic functional groups play a crucial role in the corrosion inhibition process. The XPS test results also proved the existence of corrosion inhibition film on the sample surface.

ACKNOWLEDGEMENTS

The author would like to thank Minjie Yan for his great help with SEM characterization. This work was supported by the National Natural Science Foundation of China (No. 11604204).

CONFLICT OF INTEREST

The authors declare no financial or commercial conflict of interest.

DATA AVAILABILITY STATEMENT

The data that support the findings of this study are available from the corresponding author upon reasonable request.

References

1. M. Huang, M. X. Zhang, Y. Wang, P. Zhang, A. J. Xu, *Surf Eng.*, 31 (2014) 295.
2. Q. Y. Sha, D. H. Li, *Mater. Sci. Eng., A.*, 585 (2013) 214.
3. H. B. Xue, Y. F. Cheng, *Corros. Sci.*, 53 (2011) 1201.
4. X. H. Luo, C. G. Ci, J. Li, K. D. Lin, S. Du, H. X. Zhang, X. B. Li, Y. F. Cheng, J. C. Zang, Y. L. Liu, *Corros. Sci.*, 151 (2019) 132.
5. B. Ngouné, M. Pengou, C. P. Nansou-Njiki, E. Ngameni, *Corros. Eng., Sci. Technol.*, 55 (2019)

- 138.
6. X. Wang, Y. Gu, Q. Zhang, L. L. Xu, X. Li, *Int. J. Electrochem. Sci.*, 14 (2019) 8405.
 7. L. M. P. Dolabella, T. E. D. Santos, T. Matencio, W. L. Vasconcelos, V. Lins, *Chem. Biochem. Eng. Q.*, 33 (2019) 213.
 8. Z. C. Zhang, H. J. Ba, Z. Y. Wu, Y. Zhu, *Constr. Build. Mater.*, 198 (2019) 288.
 9. Y. J. Qiang, S. T. Zhang, B. C. Tan, S. J. Chen, *Corros. Sci.*, 133 (2018) 6.
 10. Q. H. Wang, B. C. Tan, H. B. Bao, Y. T. Xie, Y. X. Mou, P. C. Li, D. B. Chen, Y. W. Shi, X. M. Li, W. J. Yang, *Bioelectrochemistry*, 128 (2019) 49.
 11. J. Tang, H. Wang, X. Q. Jiang, Z. H. Zhu, J. Xie, J. L. Tang, Y. Y. Wang, M. Chamas, Y. Q. Zhu, H. G. Tian, *Int. J. Electrochem. Sci.*, 13 (2018) 3625.
 12. R. Macedo, N. D. N. Marques, J. Tonholo, R. C. Balaban, *Carbohydr. Polym.*, 205 (2019) 371.
 13. U. Eduok, E. Ohaeri, J. Szpunar, *Electrochim. Acta*, 278 (2018) 302.
 14. K. E. Mouaden, D.S. Chauhan, M.A. Quraishi, L. Bazzi, *Sustainable Chem. Pharm.*, 15 (2020) 100213.
 15. R. Song, Z. H. Zhong, L. Lin, *Int. J. Biol. Macromol.*, 85 (2016) 102.
 16. R. Menaka, R. Geethanjali, S. Subhashini, *Mater. Today: Proc.*, 5 (2018) 16617.
 17. H. Ashassi-Sorkhabi, A. Kazempour, *Carbohydr. Polym.*, 237 (2020) 116110.
 18. V. A. Spinelli, M. C. M. Laranjeira, V. T. Fávere, *React. Funct. Polym.*, 61 (2004) 347.
 19. Y. Sangeetha, S. Meenakshi, C. Sairam Sundaram, *Int. J. Biol. Macromol.*, 72 (2015) 1244.
 20. S. A. Umoren, M. J. Banera, T. Alonso-Garcia, C. A. Gervasi, M. V. Mirífico, *Cellulose*, 20 (2013) 2529.
 21. S. A. Umoren, A. A. AlAhmary, Z. M. Gasem, M. M. Solomon, *Int. J. Biol. Macromol.*, 117 (2018) 1017.
 22. L. J. Wei, Q. Li, Y. Chen, J. J. Zhang, Y. Q. Mi, F. Dong, C. Q. Lei, Z. Y. Guo, *Carbohydr. Polym.*, 206 (2019) 493.
 23. P. P. Kong, H. X. Feng, N. L. Chen, Y. Lu, S. Y. Li, P. Wang, *RSC Adv.*, 9 (2019) 9211.
 24. M. M. Solomon, S. A. Umoren, M. A. Quraishi, M. Salman, *J. Colloid Interface Sci.*, 551 (2019) 47.
 25. M. M. Saleh, M. G. Mahmoud, H. M. Abd El-Lateef, *Corros. Sci.*, 154 (2019) 70.
 26. G. D. Cui, J. X. Guo, Y. Zhang, Q. Zhao, S. K. Fu, T. Han, S. L. Zhang, Y. H. Wu, *Carbohydr. Polym.*, 203 (2019) 386.
 27. T. Poornima, J. Nayak, A. Nityananda Shetty, *Corros. Sci.*, 53 (2011) 3688.
 28. K. R. Ansari, M. A. Quraishi, A. Singh, *Corros. Sci.*, 79 (2014) 5.
 29. M. M. Solomon, H. Gerengi, S. A. Umoren, N. B. Essien, U. B. Essien, E. Kaya, *Carbohydr. Polym.*, 181 (2018) 43.
 30. A. K. Singh, S. Mohapatra, B. Pani, *J. Ind. Eng. Chem.*, 33 (2016) 288.
 31. F. Boudjellal, H. B. Ouici, A. Guendouzi, O. Benali, A. Sehmi, *J. Mol. Struct.*, 1199 (2020) 127051.
 32. R. Sadeghi Erami, M. Amirnasr, S. Meghdadi, M. Talebian, H. Farrokhpour, K. Raeissi, *Corros. Sci.*, 151 (2019) 190.
 33. P. P. Kong, N. L. Chen, Y. Lu, H. X. Feng, J. H. Qiu, *Int. J. Electrochem. Sci.*, 14 (2019) 9774.
 34. K. G. Zhang, W. Z. Yang, X. S. Yin, Y. Chen, Y. Liu, J. X. Le, B. Xu, *Carbohydr. Polym.*, 181 (2018) 191.
 35. I. Ichchou, L. Larabi, H. Rouabhi, Y. Harek, A. Fellah, *J. Mol. Struct.*, 1198 (2019) 126898.
 36. D. S. Chauhan, K. R. Ansari, A. A. Sorour, M. A. Quraishi, H. Lgaz, R. Salghi, *Int. J. Biol. Macromol.*, 107 (2018) 1747.
 37. N. Saini, R. Kumar, H. Lgaz, R. Salghi, I.-M. Chung, S. Kumar, S. Lata, *J. Mol. Liq.*, 269 (2018) 371.
 38. F. M. Mahgoub, F. M. Al-Nowaiser, A. M. Al-Sudairi, *Prot. Met. Phys. Chem.*, 47 (2011) 381.
 39. M. A. Deyab, A. S. Fouda, M. M. Osman, S. Abdel-Fattah, *RSC Adv.*, 7 (2017) 45232.

40. W. Chen, S. Hong, H. B. Li, H. Q. Luo, M. Li, N. B. Li, *Corros. Sci.*, 61 (2012) 53.
41. X. M. Wang, Q. Wang, Y. Wan, Y. Ma, *Int. J. Electrochem. Sci.*, 11 (2016) 6229.
42. M. A. Abdo, H. A. Hassan, A. Madzlan, *Mater. Corros.*, 70 (2019) 135.
43. H. H. Zhang, X. I. Pang, K. W. Gao, *Corros. Sci.*, 157 (2019) 189.
44. Z. Sanaei, M. Ramezanzadeh, G. Bahlakeh, B. Ramezanzadeh, *J. Ind. Eng. Chem.*, 69 (2019) 18.
45. U. Eduok, E. Ohaeri, J. Szpunar, *Ind. Eng. Chem. Res.*, 58 (2019) 7179.
46. B. S. Hou, Q. H. Zhang, Y. Y. Li, G. Y. Zhu, H. F. Liu, G. A. Zhang, *Corros. Sci.*, 164 (2020) 108334.
47. C. J. Shi, X. P. Song, Y. Kan, Y. Fan, X. W. Song, Y. L. Zhang, Z. D. Zhang, *Int. J. Electrochem. Sci.*, 15 (2020) 4032.
48. Q. H. Zhang, B. S. Hou, Y. Y. Li, G. Y. Zhu, H. F. Liu, G. A. Zhang, *Corros. Sci.*, 164 (2020) 108346.
49. M. Corrales-Luna, T. Le Manh, M. Romero-Romo, M. Palomar-Pardavé, E. M. Arce-Estrada, *Corros. Sci.*, 153 (2019) 85.
50. J. Haque, V. Srivastava, D. S. Chauhan, M. A. Quraishi, A. Madhan Kumar, H. Lgaz, *Sustainable Chem. Pharm.*, 16 (2020) 100260.
51. M. R. Vinutha, T. V. Venkatesha, *Port. Electrochimica Acta.*, 34 (2016) 157.

© 2021 The Authors. Published by ESG (www.electrochemsci.org). This article is an open access article distributed under the terms and conditions of the Creative Commons Attribution license (<http://creativecommons.org/licenses/by/4.0/>).